Available online at www.sciencedirect.com

SciVerse ScienceDirect

Ceramics International 39 (2013) 8123–8131

CERAMICS INTERNATIONAL

www.elsevier.com/locate/ceramint

Effect of Sr and Ca dopants on oxidation and electrical properties of lanthanum chromite-coated AISI 430 stainless steel for solid oxide fuel cell interconnect application

Hamed Rashtchi*, Mohammad Ali Faghihi Sani, Amir Masoud Dayaghi

Department of Materials Science and Engineering, Sharif University of Technology, Azadi Avenue, P.O. Box 11155-9466 Tehran, Iran

Received 24 January 2013; received in revised form 18 March 2013; accepted 25 March 2013
Available online 10 April 2013

Abstract

Lanthanum chromite coating occupies a noticeable position as a ceramic coating on metallic interconnects in solid oxide fuel cells because of its excellent electrical conductivity, high oxidation resistance and desirable chemical stability in both oxidizing and reducing atmospheres. In the present work, a sol–gel process based on the dip-coating technique was used to prepare dense and uniform coatings on metallic alloy for interconnect application (AISI 430 type). The effect of strontium and calcium doping into lanthanum chromite structure on electrical conductivity and oxidation behavior of the coated sample has been investigated. The oxidation behavior was evaluated by cyclic oxidation test at 800 °C in lab air. In addition, the area specific resistance (ASR) of the coated and uncoated samples after long-term oxidation was measured through a two-point, four-wire probe method. It was found that, for the coated sample, when compared to the bare metallic one, the addition of Ca into lanthanum chromite coating drastically lowered the oxidation rate and electrical resistance by approximately 2 and 6 times, respectively.
© 2013 Elsevier Ltd and Techna Group S.r.l. All rights reserved.

Keywords: A. Sol–gel processes; Solid oxide fuel cells; Area specific resistance; Oxidation behavior

1. Introduction

Fuel cells are regarded as eco-friendly power sources that generate electricity through an electrochemical reaction between fuel and oxygen. Fuel cells do have manifest advantages, namely high energy conversion efficiency without harmful gaseous emission [1–3]. Among various types of fuel cells, solid oxide fuel cells (SOFCs) have extra merits, including acceptable energy output and fuel flexibility [3–6]. A single cell of the SOFCs consists of two electrodes (cathode and anode) separated by a solid oxide material acting as electrolyte. Oxygen supplied in the cathode side is combined with free electrons to form oxide ions moving to the anode through the electrolyte. At the anode side, hydrogen or monoxide carbon as fuel is fed and reacts with incoming oxygen ions from the electrolyte to form water (and/or carbon dioxide), releasing free electrons. Liberated electrons move to the cathode from an external circuit and produce electricity. In practice, a single cell cannot produce enough energy so that the output voltage may not exceed 1 V. Therefore, many cells are stacked together with interconnects [7,8]. The interconnect has two main roles: transmitting the generated electricity to the external circuit and separating the fuel and oxygen paths in the stack [6,9]. Interconnect material must satisfy some criteria, including good electrical and thermal conductivity, high density without open porosity, high creep resistance, chemical and physical stability in both oxidizing and reducing atmospheres and compatibility of its thermal expansion coefficient (TEC) with that of the other components of the cell to perform at operating temperature (between 600 °C and 800 °C) [9–11].

Due to recent progresses in reducing the SOFC operating temperature from 1000 °C to less than 800 °C, it is possible to use more economical and accessible interconnect materials instead of expensive ceramic ones [12–15]. Among the

Abbreviations: SOFC, solid oxide fuel cell; LC, lanthanum chromite; LSC, Sr-doped lanthanum chromite; LCC, Ca-doped lanthanum chromite; TEC, thermal expansion coefficient; ASR, area specific resistance; PVD, physical vapor deposition; CVD, chemical vapor deposition; TGO, thermally grown oxide

*Corresponding author. Tel.: +98 913 326 5916; fax: +98 21 6600 5717.
E-mail addresses: rashtchi@alum.sharif.edu, h.rashtchi@gmail.com (H. Rashtchi), faghihi@sharif.edu (M.A.F. Sani).

0272-8842/$ - see front matter © 2013 Elsevier Ltd and Techna Group S.r.l. All rights reserved.
http://dx.doi.org/10.1016/j.ceramint.2013.03.085

investigated alloys as interconnect materials, ferritic stainless steels (FSSs) have attracted more attention due to their superior properties such as good TEC matches with that of other cell components, low cost, chemical stability and high oxidation resistance which is caused by a chromia scale formed on the FSS at temperature around 650 °C–800 °C in both oxidizing and reducing atmospheres [3]. In ferritic alloys, increasing the Cr content enhances the oxidation resistance; so, a minimum amount of Cr content (17–20 wt%) is needed to form an oxide scale on the surface which can protect the alloy from further oxidation in high temperature application [11,16–18]. However, during long term oxidation FSSs still suffer from some shortcomings like the following:

- High growth rate of the chromia oxide scale during long-term oxidation, which may result in spallation of the oxide scale due to its TEC mismatch with that of FSS [10,17,19].
- Low electrical conductivity of FSS at high temperatures which is caused by chromia scale. Area specific resistance of chromia scale is around $1 \times 10^2\ \Omega\ cm^2$ at 800 °C, while the acceptable value of the interconnect material is less than $0.1\ \Omega\ cm^2$ [20,21].
- Chromium poisoning which is the most important drawback in using FSS as the interconnect material. In dry air at around 1000 °C, Cr_2O_3 of chromia-forming alloy can be oxidized into CrO_3 with the reaction

$$Cr_2O_3(s) + 3/2\ O_2(g) = 2\ CrO_3(g) \quad (1)$$

In the presence of water vapor, Cr_2O_3 can also transform to $CrO_2(OH)_2$ at lower temperature (around 800 °C) via the following reaction:

$$(1/2)\ Cr_2O_3(s) + (3/4)\ O_2(g) + H_2O(g) = CrO_2(OH)_2(g) \quad (2)$$

These Cr vapor species migrate into the cathode, deposit on its surface and lead to Cr poisoning at the interface of cathode and YSZ electrolyte, degrading performance of the cell [3,14,22–25].

To decrease the FSSs degradation rate, a protective layer might be applied. This protective layer must have close TEC match with the substrate and must decrease Cr migration to the cathode [9,11]. Perovskite-type oxide coatings with the general formula of ABO_3 (such as $LaCrO_3$, $LaMnO_3$, $LaCoO_3$ and $LaFeO_3$), where A is a rare earth cation (e.g., La) and B is usually a transition metal (e.g., Cr), are among the most promising protective coatings [10,11,15,26]. Among them, lanthanum chromite coating shows superior properties such as good stability in oxidizing and reducing atmospheres and desirable surface adhesion in SOFC operating temperature range from 650 °C to 800 °C [14,15,26–28]. Lanthanum chromite is a p-type conductor in oxidizing atmospheres. To increase its electrical conductivity, La can be substituted by large earth alkali cations, e.g., Sr or Ca.

Different coating techniques have been used, including plasma spray coating [29,30], laser ablation [31], chemical vapor deposition (CVD) [32,33], screen printing [34,35], electron-beam physical vapor deposition (EB-PVD) [36], RF-magnetron sputtering [37] and wet chemical techniques, to create the protective ceramic film on the substrate [9,38,39]. Among the above mentioned techniques, sol–gel route submits important privileges, namely high resulting homogeneity, low sintering temperature and low cost [11,25,40].

In this work, a perovskite-based coating, lanthanum chromite, was applied on stainless steel (AISI 430) through the sol–gel dip coating method to alleviate substrate oxidation at SOFC operating temperature. Moreover, electrical conductivity and oxidation behavior of the coated samples were investigated in lab air to understand the effect of strontium and calcium doping into the lanthanum chromite structure.

2. Experimental

2.1. Sample preparation

A commercial stainless steel plate (AISI 430) with the chemical composition given in Table 1 was used as substrate. The sheet was cut into 1 cm × 1 cm × 1 mm samples by wire cut electric device. All samples were polished with grit SiC papers from #320 to #2000 and subsequently with diamond pastes (from 0.3 to 0.05 μm). The samples were then ultrasonically cleaned in acetone and ethanol sequentially, and were dried in an oven at 100 °C.

2.2. Coating process

Starting materials used to prepare stable lanthanum chromite sols (with and without Ca or Sr dopants) were lanthanum(III) nitrate hexahydrate [$La(NO_3)\cdot 6H_2O$, MERCK, 99% pure], strontium nitrate [$Sr(NO_3)_2$, MERCK, 99.99% pure], calcium nitrate tetrahydrate [$Ca(NO_3)_2\cdot\ 4H_2O$, MERCK, 99.99% pure], chromium(III) nitrate nonahydrate [$Cr(NO_3)_3\ 9H_2O$ MERCK, 99% pure], citric acid (as a chelating agent) and distilled water (as a solvent). The total metallic ions concentration in all starting solutions was 0.6 M. In the case of the $LaCrO_3$ (LC) coating, the atomic ratio of La:Cr was 1:1 and for the $La_{0.8}Ca_{0.2}CrO_3$ (LCC) or $La_{0.8}Sr_{0.2}CrO_3$ (LSC) coatings, the atomic ratio of La:Ca (or Sr):Cr was 0.8:0.2:1.

Appropriate amounts of metallic nitrates were dissolved in 40 ml distilled water. Then, citric acid was added to the solutions. These solutions were stirred and heated at 80 °C for 24 h to prepare the sols. Subsequently, samples were immersed into the prepared sols and were removed at a constant speed of 6 cm/min. The coated samples were dried at 80 °C for 1 h and 250 °C for 30 min, sequentially. This procedure was repeated three times to build up a suitable film thickness. Finally, the coated samples were heated at 800 °C for 1 h in lab air to form the desired perovskite structure named

Table 1
Chemical composition (in wt%) of AISI 430.

Elements	Fe	Cr	Mo	Si	Mn
Composition	81.63	16.51	1.19	0.31	0.36

"as-deposited samples". The applied coatings on the as-deposited samples had the average thickness of 1.3 μm (measured with SEM image analyses software). The described procedure is summarized in Fig. 1.

2.3. Oxidation behavior

A fixed oxidation cycle was performed eight times in lab air to study the oxidation behavior of the bare and various coated samples. In each cycle, samples were heated up to 800 °C with a heating rate of 3 °C/min, were soaked at this temperature for 120 h, and finally were cooled down to 100 °C in the furnace. Then, the samples were transferred into a desiccator to prevent any moisture absorption while cooling to room temperature. So, the accumulated oxidation time was 960 h. The weight gain of the samples was recorded after each cycle using a digital balance with an accuracy of ±0.01 mg to evaluate the oxidation behavior.

2.4. Coating characterization

The perovskite-type coatings and oxide scales were characterized by an X-ray diffractometer (X'Pert MPD, Philips, equipped with beam monochromator for CuKα at 40 kV and 30 mA scanned over $2\theta = 20–70^\circ$ in steps of 0.04° and a scan speed of $1^\circ\ min^{-1}$). Morphological and elemental characterizations of the coated protective films and the thermally grown oxide (TGO) scales were also examined by scanning electron microscopy (SEM, Tescan VEGAII XMU) equipped with energy dispersive X-ray spectroscopy (EDX) at a voltage of 20 kV. Microstructural investigations and cross-sectional observations of the coatings were performed by secondary electron (SE) and back scattered electron (BSE) imaging modes, respectively. Moreover, the thickness of the formed oxide layers was measured with SEM image analyses software.

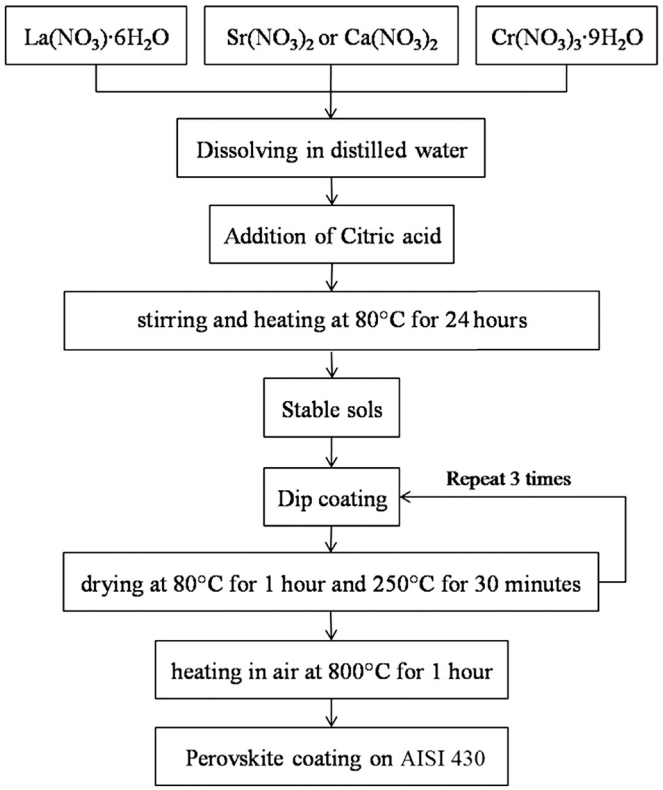

Fig. 1. Experimental guideline for perovskite coatings fabrication.

2.5. Electrical resistance

The area specific resistance (ASR) of the resulting final oxide scale (including thermally grown oxide (TGO) scale and coating) formed on the bare and coated samples after eight 120-h oxidation cycles (with a cumulative exposure time of 960 h) was measured at specified temperatures from 450 °C to 800 °C with an interval of 50 °C using a two-point, four-wire probe method. In this process, to make Pt electrodes, both sides of each oxidized sample were covered with Pt paste. Then, Pt meshes, as current collectors, as well as Pt wires were fixed on both sides. This setup was placed in a furnace. A constant current of 10 mA was passed through Pt wires and simultaneously the voltage was measured at each temperature. Finally, ASR of the resulting final oxide scale (TGO scale and coating) formed on the bare and coated samples was calculated at each specified temperature according to Ohm's law.

3. Results and discussion

3.1. Oxidation kinetics and behavior

Fig. 2 shows the oxidation behavior of the bare sample, as well as $LaCrO_3$, $La_{0.8}Sr_{0.2}CrO_3$ and $La_{0.8}Ca_{0.2}CrO_3$ coated

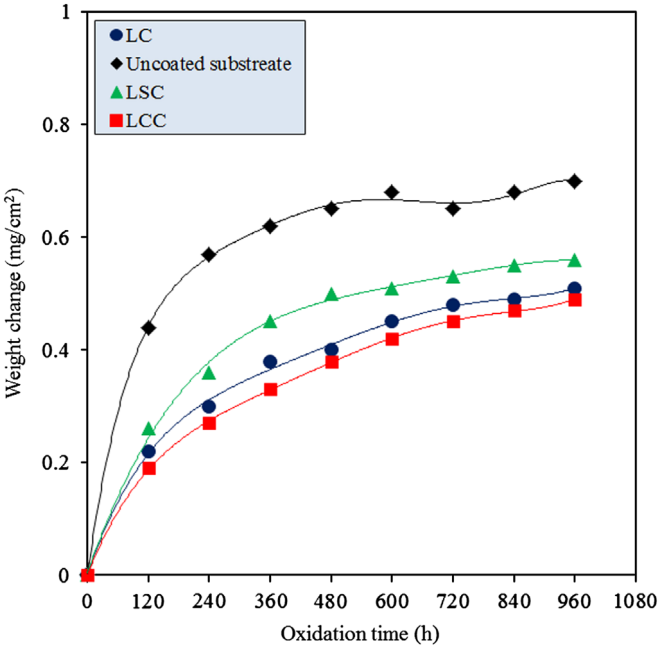

Fig. 2. Weight changes of the bare and various coated samples as a function of oxidation time during cyclic oxidation test in lab air at 800 °C for 960 h (eight 120-h cycles).

ones, during cyclic oxidation exposure (eight 120-h cycles) at 800 °C in lab air. All coated samples presented a near parabolic behavior. Considering the long term exposure, and assuming the oxidation process as diffusion controlled, according to the parabolic law, the oxide scale weight change was proportional to the square root of time [11,19,41]:

$$(\Delta W/A)^2 = K_0 t \quad (3)$$

where ΔW is the weight change, A is the sample surface area, K_0 is the parabolic oxidation rate constant and t is the oxidation time.

Based on Eq. (1) and the oxidation test results presented in Fig. 2, the parabolic rate constants of the bare and various coated samples after 960 h of oxidation were calculated and are given in Table 2. It was found that the parabolic rate constant of the Ca-doped lanthanum chromite coated sample was about two orders of magnitude lower than that of the bare one, showing the drastic effectiveness of coating in reducing the oxidation rate during cyclic oxidation exposure. These results also revealed that the LC and LCC coated samples had a somewhat similar weight gain (considering the resulting weight as TGO scale and coating), quite lower in comparison with the LSC coated sample.

3.2. Microstructural characterizations

Fig. 3 shows surface morphologies of the bare sample as well as LC, LSC and LCC coated samples after cyclic

Table 2
Parabolic oxidation rate constants of the bare and various coated substrates.

	Coating type	Oxidation parabolic rate constant (K_0) after 960 h ($g^2\ cm^{-4}\ s^{-1}$)
(1)	Uncoated substrate	1.41×10^{-13}
(2)	$LaCrO_3$ coated substrate (LC)	7.52×10^{-14}
(3)	$La_{0.8}Sr_{0.2}CrO_3$ coated substrate (LSC)	9.07×10^{-14}
(4)	$La_{0.8}Ca_{0.2}CrO_3$ coated substrate (LCC)	6.94×10^{-14}

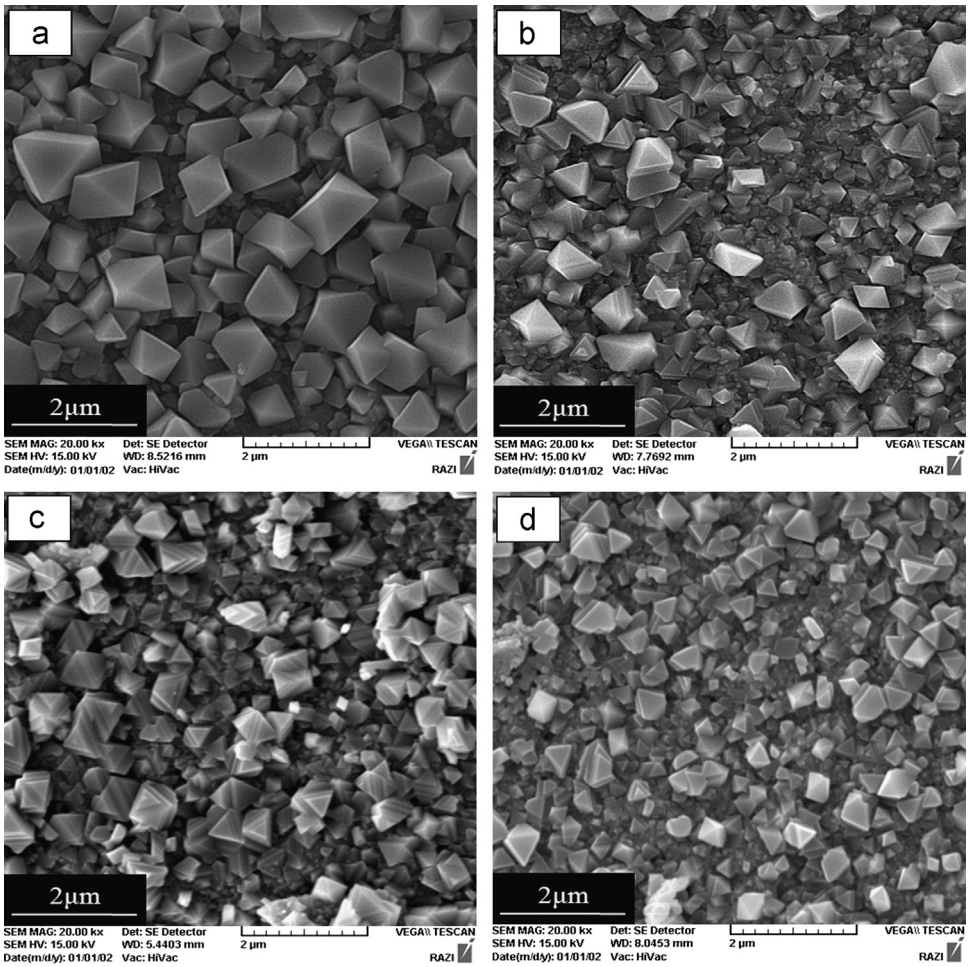

Fig. 3. Surface micrographs of (a) bare AISI 430 sample, (b) $LaCrO_3$, (c) $La_{0.8}Sr_{0.2}CrO_3$ and (d) $La_{0.8}Ca_{0.2}CrO_3$ coated AISI 430 samples, after cyclic oxidation test in lab air at 800 °C for 960 h.

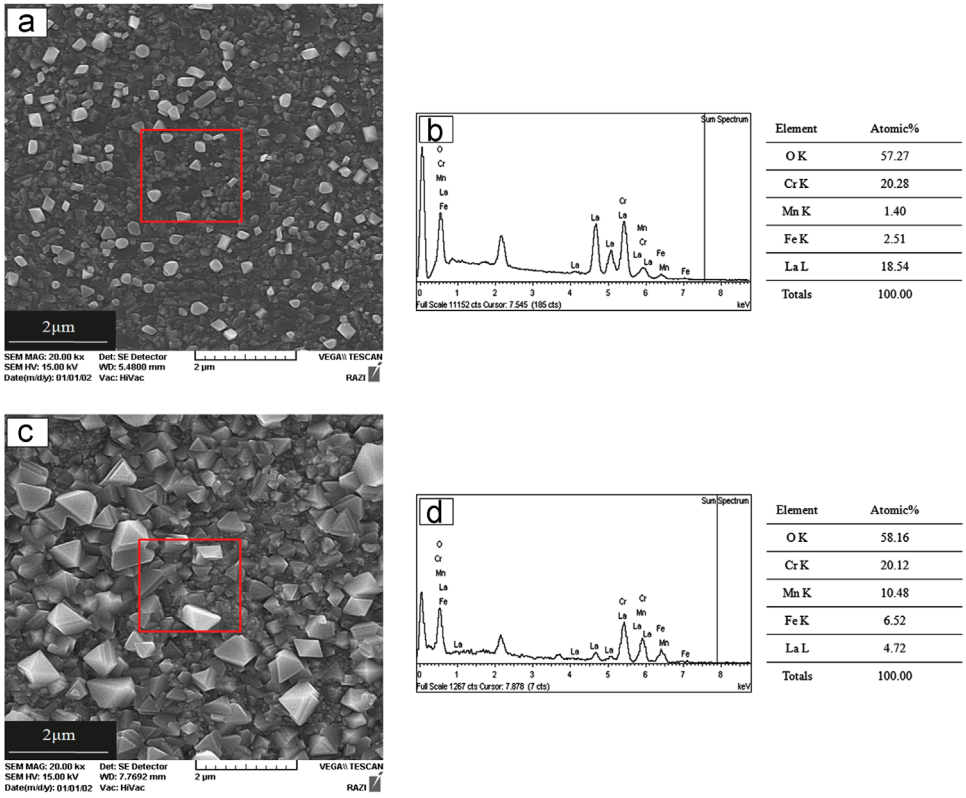

Fig. 4. Lanthanum chromite coatings: (a) morphology of as-deposited sample after heating at 800 °C for 1 h, (b) EDX result from square area marked in Fig. 5(a), (c) morphology of the $LaCrO_3$ coated sample cyclically oxidized in lab air at 800 °C for 960 h, and (d) EDX result from square area marked in Fig. 5(c).

oxidation in lab air at 800 °C for 960 h. It was found that particle size of the oxide scale formed on the bare sample was larger than that of the coated ones. Moreover, a comparison between Fig. 3(c) and (d) demonstrates that the surface of the Ca-doped $LaCrO_3$ coated sample was slightly smoother and denser than that of the Sr-doped $LaCrO_3$ coated one. The reason for this phenomenon is the formation of more porosities in the case of Sr-doped $LaCrO_3$ coated sample.

Morphologies of the $LaCrO_3$ coated samples before and after cyclic oxidation are presented in Fig. 4. Surface morphology of the as-deposited sample, Fig. 4(a), was dense with no significant porosity with an average grain size of 200–300 nm obtained by SEM image analyses software. Fig. 4(b) shows the EDX result of the square area identified in Fig. 4(a). Phase structure of the coating mainly consisted of La, Cr and O, estimated to be $LaCrO_3$. According to Fig. 4(c), an increase in grain size to about 0.6–1 μm was observed after long-term oxidation. Fig. 4(d) shows the EDX result of the square area identified in Fig. 4(c). As the EDX result shows, the grains composition mainly consisted of Mn, Cr and O with lower La concentration compared to the as-deposited sample. Fe cations were also partially diffused from the sample to the oxide layer during long-term oxidation. It must be noted that some peaks in the EDX spectra around 2.2 keV are related to the Au coating sputtered in the SEM sample preparation process.

Fig. 5 shows cross-section of the bare and perovskite coated samples after cyclic oxidation. To protect oxide layers against destruction and spallation during cross sectioning, a Cu film was applied on the oxide layers via the PVD technique. The oxide scale average thicknesses of the bare sample as well as LSC, LC and LCC coated ones were approximately 5.5, 2.5, 2 and 2 μm, respectively, measured with SEM image analyses software. These resulting thicknesses are in good agreement with the thermogravimetrical results presented in Fig. 2. The LC and LCC coated samples showed similar oxidation behavior while a higher oxidation rate was found for the LSC coated samples.

3.3. Chemical composition characterizations

Cross sectional backscattered images of the coated and uncoated samples (Fig. 5) showed that oxide scales formed during oxidation exposure comprised two different layers, a sub-layer adjacent to the sample and a top one. Fig. 6 presents the EDX analysis of two areas (a and b areas) specified in the cross sectional image of LC coated sample (Fig. 5(b)). It can be seen that the sub-layer is Cr-rich, and the top one is Mn/Cr-rich. Cr and Mn ions partially diffuse from the sample through the oxide layers, forming Mn–Cr spinel faceted particles above the film observed in Fig. 3. From EDX results, the Mn/Cr atomic ratio of the spinel top layer is approximately 1/2. So, the spinel structure is most likely $MnCr_2O_4$.This is also confirmed with XRD results in Fig. 8. The same results, not shown here, were obtained for the bare sample as well as LCC and LSC coated ones. By comparing the thickness of oxide scale (TGO and coating) formed on the bare and coated samples (Fig. 5), it was found that the oxide scale

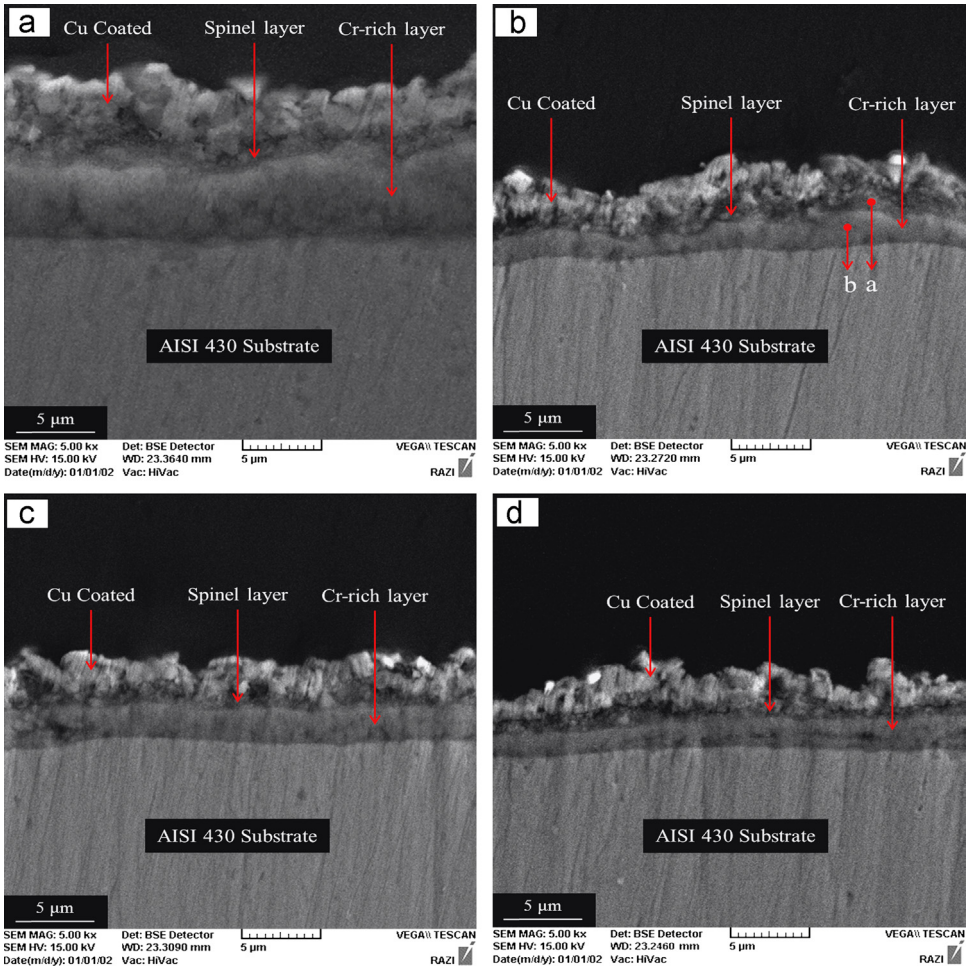

Fig. 5. Cross-sectional backscattered electron micrographs of (a) bare AISI 430 sample, (b) $LaCrO_3$, (c) $La_{0.8}Sr_{0.2}CrO_3$ and (d) $La_{0.8}Ca_{0.2}CrO_3$ coated AISI 430 samples, after cyclic oxidation test in lab air at 800 °C for 960 h.

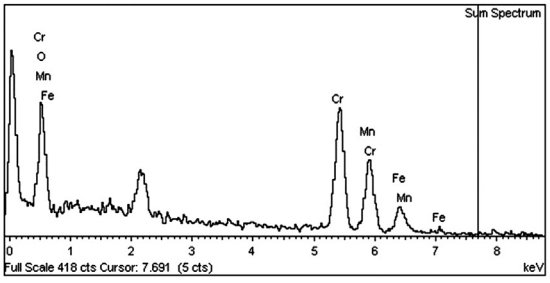

$MnCr_2O_4$ layer — a

Element	Atomic%
O K	64.67
Cr K	20.05
Mn K	10.50
Fe K	4.78
Totals	100.00

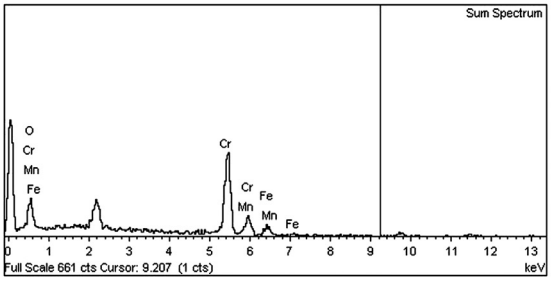

Cr_2O_3 layer — b

Element	Atomic%
O K	55.99
Cr K	35.94
Mn K	2.89
Fe K	5.18
Totals	100.00

Fig. 6. EDX results given from the two areas (a and b areas) marked in cross section image in Fig. 5(b).

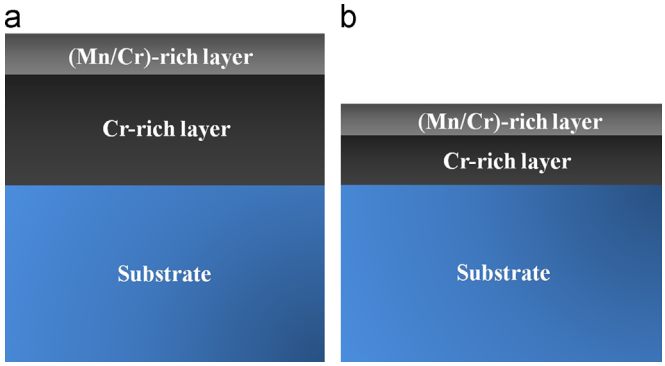

Fig. 7. Schematic of thermally-grown oxide layers formed on AISI 430 after cyclic oxidation test in lab air at 800 °C for 960 h: (a) uncoated and (b) coated samples.

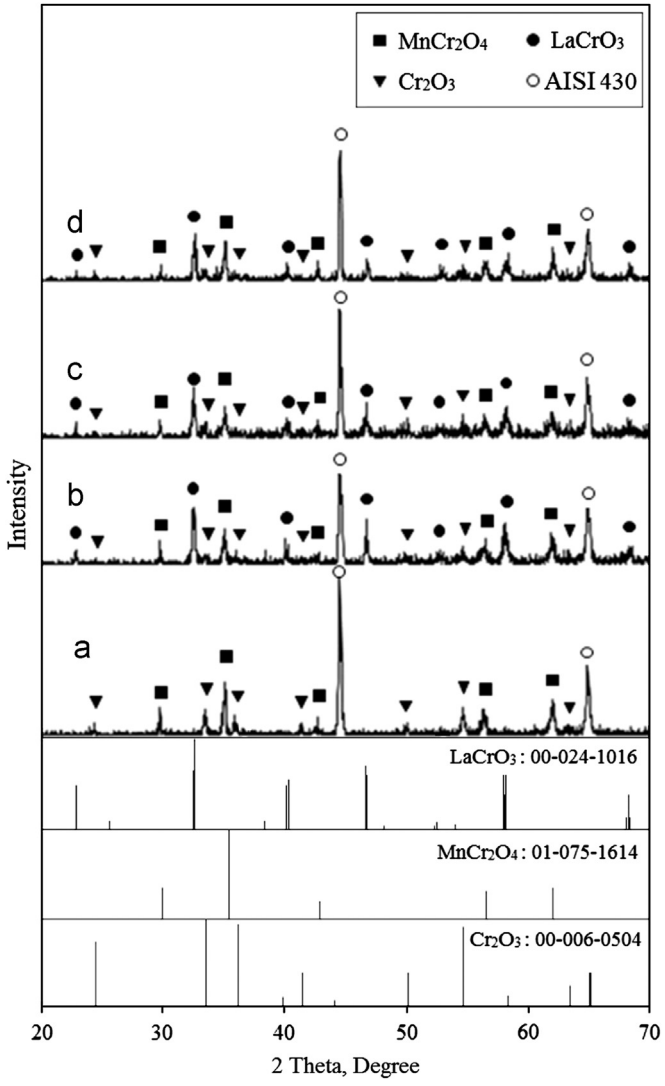

Fig. 8. XRD patterns of (a) bare AISI 430, (b) $LaCrO_3$, (c) $La_{0.8}Sr_{0.2}CrO_3$ and (d) $La_{0.8}Ca_{0.2}CrO_3$ coated AISI 430 samples, after cyclic oxidation test in lab air at 800 °C for 960 h.

formed on the bare sample was thicker. So, it can be concluded that the Cr-rich scale formed on the bare sample predominantly has grown considerably during the thermal cycling test in

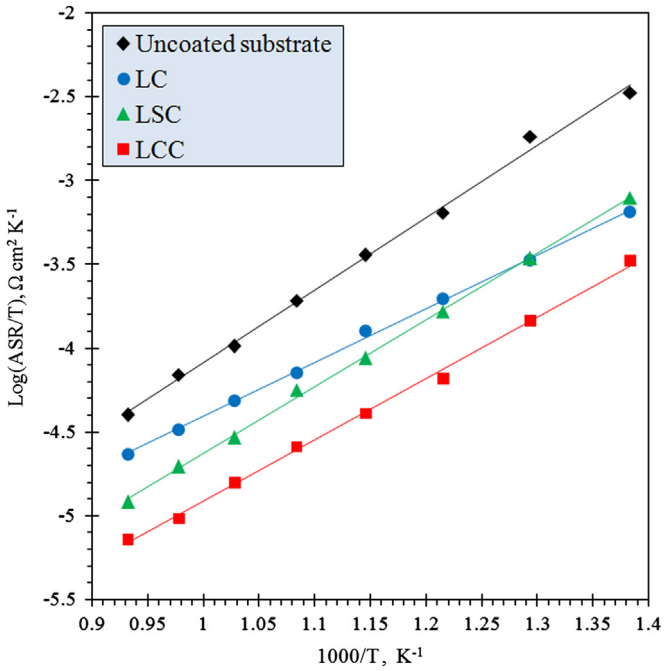

Fig. 9. Area specific resistance of the bare and various coated samples as a function of temperature after cyclic oxidation test in lab air at 800 °C for 960 h.

comparison to the perovskite coated ones, presenting high efficiency of protective perovskite coatings in retarding Cr outward diffusion which has been demonstrated by other authors [9,11,16,26,27]. On the other hand, the Mn–Cr spinel layer formed on the coated samples after thermal exposure is desirable for SOFC application. This is because the $MnCr_2O_4$ facilitates the electrical conductivity of the interconnect and extenuates the Cr evaporation [14,16]. After long-term exposure (960 h), no distinctive perovskite layer was observed in the cross-sectional images of the coated samples. This is possibly due to partial dissolution of the $LaCrO_3$ layer in the oxide scale (TGO) during thermal cyclic exposure as mentioned in literature [11,14]. In other words, $LaCrO_3$ and the formed oxide like Cr_2O_3 could possibly disslove in each other and no separable interface can be recognized between $LaCrO_3$ coating and TGO. Formation of different oxide layers on the bare and LC coated samples after cyclic oxidation exposure is schematically shown in Fig. 7.

XRD patterns of the bare and various coated samples after cyclic oxidation test are presented in Fig. 8. Alongside well defined peaks of AISI 430, chromia and Mn–Cr spinel peaks were evident in all samples. For coated samples, lanthanum content perovskite peaks were also observed. Although peaks of $MnCr_2O_4$ and Cr_2O_3 were detected in all samples, the intensity of the chromia main peak was somehow lower in the cases of the coated samples in comparison with the bare one, due to the presence of perovskite coatings. Although the presence of perovskite coatings can mitigate the chromia layer growth, considering that $MnCr_2O_4$ and Cr_2O_3 layers were formed on all the samples (uncoated and coated samples) during oxidation, the Cr-rich layer growth cannot be completely stopped, as reported by other researchers [10,16,26]. Cross sectional images and XRD results (Figs. 5 and 8, respectively)

imply that the LCC coating layer was the most effective barrier to reduce the oxygen penetration rate from atmosphere to the sample surface. Among various coating layers, the LSC one (with the highest porosity) has the highest oxygen diffusion rate. The highest level of porosity in the LSC coating layer is due to formation of intermediate $SrCrO_4$ phase during heat treating of primary gel film at lower temperatures (around 600 °C) and its further decomposition to $SrCrO_3$ and oxygen at elevated temperatures (around 700 °C) [42]. In fact, the formed gaseous oxygen can leave pores during its escape from the coating [2,26].

3.4. Electrical resistance of the coated samples

One of the most important criteria of interconnect playing a critical role in SOFC applications is its electrical resistance. Fig. 9 presents the log(ASR/T) of bare and various coated samples versus $10^3/T$ after cyclical oxidation test. It is assumed that the electrical resistance of metallic substrate is negligible compared to that of the oxide scale; therefore, the measured ASR is related only to the oxide scale and its interfaces with the alloy and Pt electrodes. Since the constant current used in the two-point, four-wire probe approach is low (10 mA), the interfacial polarization can be neglected [19]. So, the measured ASR presents electrical resistance of the oxide scale only. From Fig. 9, it can be seen, for all samples, that there was a linearly upward trend in log(ASR/T) as the temperature decreases, which is in accordance with the Arrhenius equation:

$$\mathrm{ASR}/T = A\ exp(E_a/kT) \quad (4)$$

where A is an exponential constant, E_a is the activation energy and k is the Boltzmann constant. At 800 °C, the ASR values of the bare sample as well as LC, LSC and LCC coated ones were 0.043 Ω cm^2, 0.025 Ω cm^2, 0.013 Ω cm^2 and 0.007 Ω cm^2, respectively. Among all the samples, the bare one had the highest electrical resistance while the coated ones showed much lower resistance. This clearly illustrates the drastic effect of the perovskite coating in improvement of electrical conductivity of FSS samples. Among the coated samples, the LCC coated one showed the lowest electrical resistance while the LSC coated sample presented an ASR value almost similar to that of the LC coated one. Generally, doping alkaline-earth elements, specially Sr and Ca, inside $LaCrO_3$ structure improves the electrical conductivity. This is due to formation of electron holes, resulting from transition of Cr^{3+} to Cr^{4+} to compensate negative charges posed by substitution of Sr^{2+} or Ca^{2+} at La^{3+} sites [17,19]. The differences in ASR values between LSC and LCC coated samples can be related to the cell volume difference between $La_{0.8}Sr_{0.2}CrO_3$ and $La_{0.8}Ca_{0.2}CrO_3$. Considering ionic radii of La^{3+}, Ca^{2+} and Sr^{2+} (1.17 Å, 1.14 Å and 1.32 Å, respectively), the Ca doping causes less lattice distortion than Sr doping inside $LaCrO_3$ structure because Ca^{2+} radius is closer to the La^{3+} one. The mentioned lattice distortion causes strain and degrades the conductivity [43].

In the present study, although applying the lanthanum chromite coatings (with and without dopant) on FSS as interconnect material showed promising properties in lab air, such coatings need further investigations. They are stable in an oxidizing atmosphere, but in a reducing one, the electrical properties are weaker. Moreover, TEC of these coatings depends on the oxygen partial pressure. So, for SOFC interconnect applications, more tests are needed to evaluate the actual performance of the lanthanum chromite coated AISI 430 such as testing in dual atmosphere exposure with SOFC electrodes and seal contacts.

4. Conclusion

Uniform perovskite films with and without Sr or Ca dopants were successfully coated on AISI 430 sample through the sol–gel dip coating technique. Oxidation behavior of the bare and various coated samples was evaluated using cyclic oxidation test. All samples were oxidized during eight 120-h cycles (totally 960 h) at 800 °C in lab air atmosphere. The perovskite coatings effectively improved oxidation behavior of the AISI 430 sample, inhibited surface oxide grain growth as well as oxide scale thickness during the oxidation process and reduced Cr diffusion. However, outward diffusion of Cr species was not completely suppressed. A parabolic behavior was observed for all coated samples during cyclic oxidation exposure. No surface spallation occurred for the coated samples. Moreover, Ca-doped lanthanum chromite coated sample presented the highest oxidation resistance and the lowest parabolic oxidation rate constant, about half of the bare sample. Area specific resistances of the bare and various coated samples were also measured through a two-point, four-wire probe method. The electrical conductivity of lanthanum chromite coating increased by adding Ca and Sr dopants. However, the Ca-doped $LaCrO_3$ coated sample showed the highest conductivity.

Acknowledgments

The authors would like to thank the Iran Renewable Energy Organization (SUNA) for the financial support of this research. Moreover, the authors wish to acknowledge Dr. Zigui Lu at Pacific Northwest National Laboratory of the US Department of Energy for helpful discussions during the course of this work.

References

[1] Q.M. Nguyen, T. Takahashi, Science and Technology of Ceramic Fuel Cells, Elsevier Science, New York, USA, 1995.
[2] H. Bhatt, J. Bahadur, M.N. Deo, S. Ramanathan, K.K. Pandey, D. Sen, S. Mazumder, S.M. Sharma, Effects of calcination on microscopic and mesoscopic structures in Ca- and Sr-doped nano-crystalline lanthanum chromites, Journal of Solid State Chemistry 184 (2011) 204–213.
[3] J.W. Fergus, R. Hui, X. Li, D.P. Wilkinson, J. Zhang, Solid Oxide Fuel Cells: Materials Properties and Performance, CRC Press, Boca Raton, FL, USA, 2009.
[4] K. Eguchi, H. Kojo, T. Takeguchi, R. Kikuchi, K. Sasaki, Fuel flexibility in power generation by solid oxide fuel cells, Solid State Ionics 152–153 (2002) 411–416.
[5] B.C.H. Steele, A. Heinzel, Materials for fuel-cell technologies, Nature 414 (2001) 345–352.

[6] R.P. O'Hayre, S.W. Cha, W. Colella, Fuel Cell Fundamentals, John Wiley & Sons, Hoboken, New Jersey, USA, 2009.
[7] Z. Yang, S.C. Singhal, Fuel Cells—Solid Oxide Fuel Cells | Cell Interconnection, Encyclopedia of Electrochemical Power Sources, Elsevier, Amsterdam63–76.
[8] High-temperature solid oxide fuel cells: fundamentals, design and applications, Materials Today 5 2002 55.
[9] J.H. Zhu, Y. Zhang, A. Basu, Z.G. Lu, M. Paranthaman, D.F. Lee, E. A. Payzant, $LaCrO_3$-based coatings on ferritic stainless steel for solid oxide fuel cell interconnect applications, Surface and Coatings Technology 177–178 (2004) 65–72.
[10] J.S. Yoon, J. Lee, H.J. Hwang, C.M. Whang, J.W. Moon, D.H. Kim, Lanthanum oxide-coated stainless steel for bipolar plates in solid oxide fuel cells (SOFCs), Journal of Power Sources 181 (2008) 281–286.
[11] Z. Lu, J. Zhu, Y. Pan, N. Wu, A. Ignatiev, Improved oxidation resistance of a nanocrystalline chromite-coated ferritic stainless steel, Journal of Power Sources 178 (2008) 282–290.
[12] T. Kadowaki, T. Shiomitsu, E. Matsuda, H. Nakagawa, H. Tsuneizumi, T. Maruyama, Applicability of heat resisting alloys to the separator of planar type solid oxide fuel cell, Solid State Ionics 67 (1993) 65–69.
[13] T. Brylewski, M. Nanko, T. Maruyama, K. Przybylski, Application of Fe–16Cr ferritic alloy to interconnector for a solid oxide fuel cell, Solid State Ionics 143 (2001) 131–150.
[14] W.J. Shong, C.K. Liu, C.Y. Chen, C.C. Peng, H.J. Tu, G.T.K. Fey, R. Y. Lee, H.M. Kao, Effects of lanthanum-based perovskite coatings on the formation of oxide scale for ferritic SOFC interconnect, Materials Chemistry and Physics 127 (2011) 45–50.
[15] Z.J. Feng, C.L. Zeng, $LaCrO_3$-based coatings deposited by high-energy micro-arc alloying process on a ferritic stainless steel interconnect material, Journal of Power Sources 195 (2010) 4242–4246.
[16] J.S.Y. Eun, A. Lee, Hae Jin Hwang, Ji-Woong Moon, Nam-ung Cho, Consumptive coating layer synthesis by a sol–gel technique on a stainless steel substrate for an IT-SOFC separator, Journal of Ceramic Processing Research 9 (2008) 538–543.
[17] W.Z. Zhu, S.C. Deevi, Development of interconnect materials for solid oxide fuel cells, Materials Science and Engineering A 348 (2003) 227–243.
[18] Z. Lu, Electrically Conductive Spinel and Perovskite Phases for Solid Oxide Fuel Cell Interconnect Application, Doctor of Philosophy, Tennessee Technological University, 2005.
[19] K. Huang, P.Y. Hou, J.B. Goodenough, Characterization of iron-based alloy interconnects for reduced temperature solid oxide fuel cells, Solid State Ionics 129 (2000) 237–250.
[20] G.V. Samsonov, The Oxide Handbook, IFI/Plenum, 1982.
[21] W.Z. Zhu, S.C. Deevi, Opportunity of metallic interconnects for solid oxide fuel cells: a status on contact resistance, Materials Research Bulletin 38 (2003) 957–972.
[22] M.C. Tucker, H. Kurokawa, C.P. Jacobson, L.C. De Jonghe, S.J. Visco, A fundamental study of chromium deposition on solid oxide fuel cell cathode materials, Journal of Power Sources 160 (2006) 130–138.
[23] H. Tu, U. Stimming, Advances, aging mechanisms and lifetime in solid-oxide fuel cells, Journal of Power Sources 127 (2004) 284–293.
[24] A. Weber, E. Ivers-Tiffée, Materials and concepts for solid oxide fuel cells (SOFCs) in stationary and mobile applications, Journal of Power Sources 127 (2004) 273–283.
[25] A.M. Dayaghi, M. Askari, H. Rashtchi, P. Gannon, Fabrication and high-temperature corrosion of sol–gel Mn/Co oxide spinel coating on AISI 430, Surface and Coatings Technology 223 (2013) 110–114.
[26] E.A Lee, S. Lee, H.J. Hwang, J.W. Moon, Sol–gel derived $(La_{0.8}M_{0.2})CrO_3$ (M=Ca, Sr) coating layer on stainless-steel substrate for use as a separator in intermediate-temperature solid oxide fuel cell, Journal of Power Sources 157 (2006) 709–713.
[27] H. Buscail, C. Issartel, F. Riffard, R. Rolland, S. Perrier, A. Fleurentin, C. Josse, Effect of various lanthanum sol–gel coatings on the 330Cb (Fe–35Ni–18Cr–1Nb–2Si) oxidation at 900 °C, Applied Surface Science 258 (2011) 678–686.
[28] L.F.G. Setz, I. Santacruz, M.T. Colomer, S.R.H. Mello-Castanho, R. Moreno, Fabrication of Sr- and Co-doped lanthanum chromite interconnectors for SOFC, Materials Research Bulletin 46 983–986.
[29] W.J. Quadakkers, H. Greiner, M. Hänsel, A. Pattanaik, A.S. Khanna, W. Malléner, Compatibility of perovskite contact layers between cathode and metallic interconnector plates of SOFCs, Solid State Ionics 91 (1996) 55–67.
[30] L.J.H. Kuo, S.D. Vora, S.C. Singhal, Plasma spraying of lanthanum chromite films for solid oxide fuel cell interconnection application, Journal of the American Ceramic Society 80 (1997) 589–593.
[31] A. Kajimura, H. Sasaki, S. Otoshi, M. Suzuki, C. Kurusu, N. Sugiura, M. Ippommatsu, Preparation of $La(Sr)CrO_{3-\delta}$ thin film interconnector by high deposition rate laser ablation method, Solid State Ionics 82 (1995) 107–111.
[32] S. Fontana, R. Amendola, S. Chevalier, P. Piccardo, G. Caboche, M. Viviani, R. Molins, M. Sennour, Metallic interconnects for SOFC: characterisation of corrosion resistance and conductivity evaluation at operating temperature of differently coated alloys, Journal of Power Sources 171 (2007) 652–662.
[33] G. Cabouro, G. Caboche, S. Chevalier, P. Piccardo, Opportunity of metallic interconnects for ITSOFC: Reactivity and electrical property, Journal of Power Sources 156 (2006) 39–44.
[34] X. Montero, N. Jordan, J. Piron-Abellan, F. Tietz, D. Stover, M. Cassir, I. Villarreal, Spinel and perovskite protection layers between crofer22-APU and $La_{0.8}Sr_{0.2}FeO_3$ cathode materials for SOFC interconnects, Journal of the Electrochemical Society 156 (2009) B188–B196.
[35] Z. Yang, G.G. Xia, X.H. Li, J.W. Stevenson, $(Mn,Co)_3O_4$ spinel coatings on ferritic stainless steels for SOFC interconnect applications, International Journal of Hydrogen Energy 32 (2007) 3648–3654.
[36] N. Oishi, T. Namikawa, Y. Yamazaki, Oxidation behavior of an La-coated chromia-forming alloy and the electrical property of oxide scales, Surface and Coatings Technology 132 (2000) 58–64.
[37] C. Johnson, R. Gemmen, N. Orlovskaya, Nano-structured self-assembled $LaCrO_3$ thin film deposited by RF-magnetron sputtering on a stainless steel interconnect material, Composites Part B: Engineering 35 (2004) 167–172.
[38] K. Huang, P.Y. Hou, J.B. Goodenough, Reduced area specific resistance for iron-based metallic interconnects by surface oxide coatings, Materials Research Bulletin 36 (2001) 81–95.
[39] W. Qu, J. Li, D.G. Ivey, Sol–gel coatings to reduce oxide growth in interconnects used for solid oxide fuel cells, Journal of Power Sources 138 (2004) 162–173.
[40] A.M. Dayaghi, M. Askari, P. Gannon, Pre-treatment and oxidation behavior of sol–gel Co coating on 430 steel in 750 °C air with thermal cycling, Surface and Coatings Technology 206 (2012) 3495–3500.
[41] B. Hua, Y. Kong, F. Lu, J. Zhang, J. Pu, J. Li, The electrical property of $MnCo_2O_4$ and its application for SUS 430 metallic interconnect, Chinese Science Bulletin 55 3831–3837.
[42] M. Mori, Y. Hiei, N.M. Sammes, Sintering behavior of Ca- or Sr-doped $LaCrO_3$ perovskites including second phase of $AECrO_4$ (AE=Sr, Ca) in air, Solid State Ionics 135 (2000) 743–748.
[43] S.P. Jiang, L. Liu, K.P. Ong, P. Wu, J. Li, J. Pu, Electrical conductivity and performance of doped $LaCrO_3$ perovskite oxides for solid oxide fuel cells, Journal of Power Sources 176 (2008) 82–89.